IEEE Access
Multidisciplinary | Rapid Review | Open Access Journal

Received July 11, 2019, accepted August 5, 2019, date of publication August 13, 2019, date of current version August 27, 2019.

Digital Object Identifier 10.1109/ACCESS.2019.2935188

Multi-Objective Optimization of Energy Management Strategy on Hybrid Energy Storage System Based on Radau Pseudospectral Method

YANWEI LIU[1], ZHENYE LI[1], ZIYUE LIN[1], KEGANG ZHAO[2], AND YUNXUE ZHU[3]

[1]School of Electromechanical Engineering, Guangdong University of Technology, Guangzhou 511006, China
[2]National Local Engineering Laboratory of Automobile Parts Technology, South China University of Technology, Guangzhou 510640, China
[3]The Fifth Electronics Research Institute of the Ministry of Industry and Information Technology, Guangzhou 510610, China

Corresponding author: Kegang Zhao (kgzhao@scut.edu.cn)

This work was supported in part by the National Natural Science Foundation of China under Grant 51575189, and in part by the Foundation of Guangdong Provincial Natural Science under Grant 2016A030313517.

ABSTRACT In this study, a multi-objective optimization method based on the Radau pseudospectral method is proposed for the energy management strategy in the hybrid energy storage system (HESS). In the proposed method, by approximating state and control variables in the system with global interpolating polynomials, the optimal control problem (OCP) is transformed into a nonlinear programming problem (NLP) and solved by a sparse nonlinear optimizer. Further, the Pareto solution set is obtained by taking the energy consumption of the HESS and the equivalent life of the battery as objective functions. Three solutions representing different tradeoffs were selected for comparative analysis: minimum system energy consumption (5819.60 kJ), with battery life 68368 cycles; maximum battery life (76227 cycles), with energy consumption 5865.68 kJ; and the balanced tradeoff optimal solution with battery life 72488 cycles and energy consumption 5841.96 kJ. The results showed that for every additional 5 kJ in system energy consumption, the battery Ah-throughput was reduced by 0.053 Ah and its equivalent life extended by 876 cycles. Further, compared with the single-cell energy source, the balanced tradeoff optimal solution increased the battery life by 29.92% and decreased the system energy consumption by 1.79%. Thus, this work provides a fast and stable multi-objective optimization method for the energy management strategy of HESS and lays the foundation for obtaining optimal system parameters.

INDEX TERMS Energy management strategy, hybrid energy storage system, multi-objective optimization, Radau pseudospectral method.

I. INTRODUCTION

Although traditional petroleum fueled vehicles have brought convenience and comfort to human life, they have also led to an energy crisis with significant environmental repercussions. A viable alternative to fossil fuel-based vehicles is electric vehicles, which provide advantages such as zero emission and low noise and can significantly reduce our consumption of fossil fuel-based energy. However, to maximize the advantages, electric vehicles require a high energy density and high power density electric energy storage system to guarantee adequate driving range and power performance. Although batteries have high energy density, their power density is low, and they also suffer from relatively short service life. However, the power density of an ultracapacitor is very high, and its service life is very long, but its energy density is low. Therefore, a hybrid energy storage system (HESS) that can fully utilize the advantages of the above two equipment by improving the energy utilization ratio and power performance of the vehicle to extend the range of the electric vehicle's mileage has been developed.

In general, the energy management strategy of the HESS has significant repercussions on the economy, power performance, and battery life of an electric vehicle. This is because there are significant differences between the dynamic characteristics and working modes of a battery compared to an ultracapacitor. Therefore, researchers worldwide have conducted extensive studies to develop an effective energy

The associate editor coordinating the review of this article and approving it for publication was Arup Kumar Goswami.

management strategy. For example, the multi-objective non-dominated sorting genetic algorithm II (NSGA-II) has been used to optimize the parameter matching and energy management strategy of hybrid power electric vehicles (EVs) [1], [2]. Convex optimization and three-level wavelet transform (WT) algorithms have also been used to match the parameters of the HESS and optimize the energy management strategy [3]–[5]. Lu *et al.* have also implemented a weighted method and a no-preference method simultaneously to transform the multi-objective optimization problem into a uni-objective convex optimization problem for hybrid energy management systems [6]. The literature shows that several studies have adopted model predictive control [7], [8], rule-based control strategies, dynamic programming algorithms [9]–[11], the projection operator adaptive law [12], and fuzzy logic control [13] to optimize the energy management strategy of HESS. However, in all these studies, the internal resistance characteristics of the battery during charge and discharge are seldom considered in the simulation process. Additionally, the optimization result does not correspond to the real word scenario, because the penalty factor that results in the reduction of the battery life is not incorporated into the battery life model to avoid the discharge of the battery with large current that degrades the service life.

Reviewing the studies cited above, we found the following drawbacks: The convergence rate of a genetic algorithm is slow, which renders it easily susceptible to fall into the local optimum. Convex optimization requires convexification in application, which is difficult to apply to practical problems. As regards dynamic programming algorithms, their computational complexity is high, and the accuracy of the solution depends on the density of the network grid. Model prediction methods and rule-based control strategies are highly sensitive to the prediction information accuracy. Further, although fuzzy logic control has strong real-time performance, it cannot guarantee the global optimum.

It should be noted that energy management optimization of the HESS has the characteristics of strong nonlinearity, multimodality, etc. Among the energy management optimization methods of the HESS currently in use, the pseudospectral method, as a global optimization method, has the advantages of fast convergence speed, large convergence radius, low initial sensitivity, and high accuracy. Moreover, its optimization result must be the global optimum [14], [15]. For example, the Legendre pseudospectral method has been used to optimize the shift process of a two-speed transmission with no power interruption [16]. Further, a pseudospectrum algorithm has been used to optimize hybrid electric vehicle (HEV) power management for fuel economy [17]. Researchers have also utilized the Gauss pseudospectrum method to develop an optimal shift strategy for a four-gear mechanical transmission electric vehicle [18]. In addition, the energy management strategy of a tandem tracked vehicle has been optimized using the Radau pseudospectrum method [15].

In this work, the internal resistance characteristics of the HEV with semi-active battery terminal load configuration are studied considering the charge and discharge characteristics of the battery. The objective function takes into account the system energy consumption and battery lifetime of the HESS. Further, the energy management strategy of the hybrid power electric vehicle is optimized via the Radau pseudospectral method, with the vehicle performance and the parameters of the battery and the capacitance as constraints.

II. HYBRID ENERGY STORAGE SYSTEM MODEL

A. HYBRID ENERGY STORAGE SYSTEM TOPOLOGY

A HESS has three configurations—passive, semi-active, and full active. In the passive HESS configuration, the battery and the ultracapacitor are connected directly in parallel with the DC busbar. This configuration has the advantage of simple structure and low cost; however, the current cannot be controlled during operation. In contrast, the fully active configuration is characterized by the adoption of two DC/DC converters with complex structure and control; however, the configuration cost is prohibitive. In the semi-active configuration, the battery or ultracapacitor is connected to the busbar via a DC/DC converter. The current can be controlled by the DC/DC converter, and the flexibility of the HESS is guaranteed. However, when the load is connected with the ultracapacitor terminal, the DC high voltage busbar is directly connected to the ultracapacitor, which leads to significant fluctuation in the voltage range that is difficult to control. In contrast, when the battery terminal is connected to the load, the system is easier to control, and the total line voltage is more stable, thereby reducing the system cost. Therefore, this study utilized a semi-active HESS battery terminal load configuration. Fig. 1 shows the topological structure of the configuration.

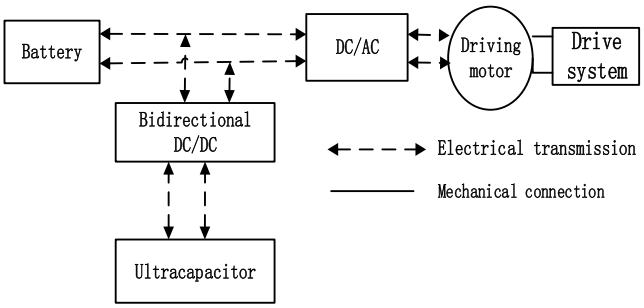

FIGURE 1. Semi-active HESS battery terminal load configuration.

B. BATTERY MODELS

As shown in Fig. 2, the single-cell model of the battery employs the internal resistance model.

In Fig 2, u_b is the open-circuit voltage of the battery; u_{b0} is the terminal voltage of the battery; i_b is the current of the battery (positive discharge and negative charge); and R_b is the equivalent series internal resistance of the battery. The battery state of charge (BSOC) is calculated via Ah-Integration:

$$BSOC(t) = BSOC(t_0) - \frac{\int i_b(t)dt}{Q_b} \tag{1}$$

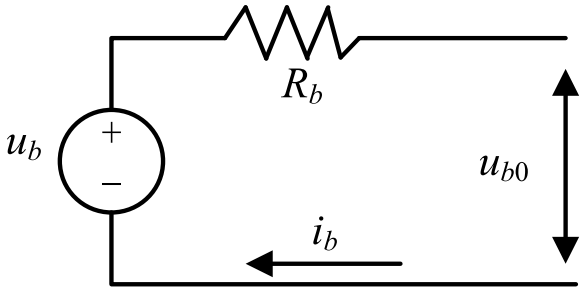

FIGURE 2. Equivalent model of power battery unit.

where BSOC (t_0) is the value of the initial BSOC, Q_b is the battery capacity, and the power of the battery is given by:

$$\begin{cases} u_{b0} = u_b(BSOC(t)) - i_b(t)^* R_b(BSOC(t)) \\ P_{b,out}(t) = i_b(t) u_{b0} \end{cases} \tag{2}$$

In (2), when $P_{b,out}$ is positive, the battery is in discharge state; Conversely, when $P_{b,out}$ is negative, the battery is in charge state. As shown in Fig. 3, the open-circuit voltage u_b is nonlinear to the charged state BSOC. Moreover, the value of internal resistance R_b is related to its charge and discharge state, as shown in Fig. 4.

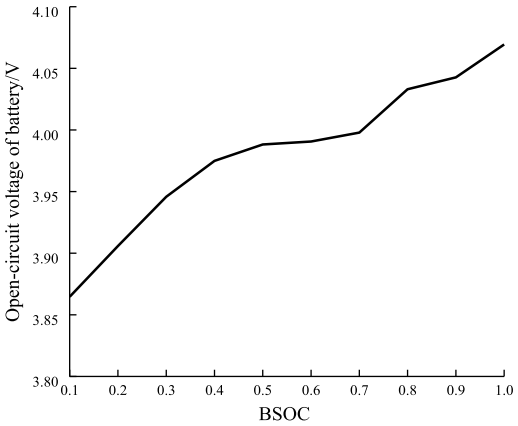

FIGURE 3. Relationship between the open-circuit voltage of the battery and BSOC.

C. ULTRACAPACITOR MODEL

Fig. 5 illustrates the monomer model of the ultracapacitor. In the figure, u_c is the open-circuit voltage of the ultracapacitor, u_{c0} is the terminal voltage, i_c is the current (positive discharge, negative charge), and R_c is the equivalent series internal resistance. The ultracapacitor state of charge (USOC) is calculated as follows:

$$USOC(t) = USOC(t_0) - \frac{\int i_c(t)dt}{C_c u_{c\max}} \tag{3}$$

where USOC (t_0) is the initial value of the USOC, C_c is the capacity of the ultracapacitor, and u_{cmax} is the maximum voltage of the ultracapacitor. The power of the ultracapacitor

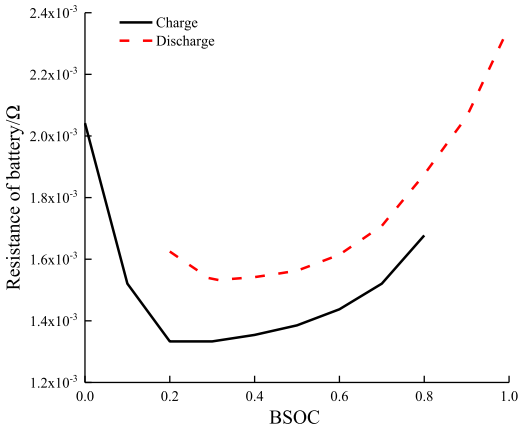

FIGURE 4. Relationship between charge and discharge resistance of the battery and BSOC.

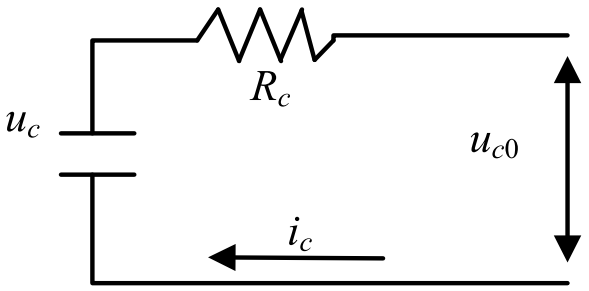

FIGURE 5. Equivalent circuit model of the ultracapacitor monomer.

is given as follows:

$$\begin{cases} u_{c0} = u_c(USOC(t)) - i_c(t)^* R_c \\ P_{c,out}(t) = i_c(t) u_{c0} \end{cases} \tag{4}$$

In (4), when $P_{c,out}$ is positive, the ultracapacitor is in the discharge state. Conversely, when $P_{c,out}$ is negative, the ultracapacitor is in the charge state. The open-circuit voltage u_c of the ultracapacitor is linear to the USOC. Therefore, energy E_c of the ultracapacitor can be expressed as follows:

$$\begin{cases} USOC(t) = \frac{u_c(t)}{u_{c\max}} \\ E_c = 0.5 C_c u_{c\max}^2 USOC^2(t) \end{cases} \tag{5}$$

D. DRIVING MOTOR MODEL

The electrical machine in the HESS functions as a motor in the driving state, and as a generator in the braking state to recover kinetic energy. In this paper, only the input and output characteristics of the motor model are considered for modeling, and the complex physical process inside the motor model is ignored. The working efficiency of the motor depends solely on the output speed and torque. Therefore, to solve the follow-up optimal control problem for energy management, normalization of the motor's speed and torque must be performed before fitting. The efficiency of the motor can be expressed by two-dimensional five-degree polynomial

fitting, as shown in (6):

$$\eta(T,n)=\sum_{i=0}^{5}\sum_{j=0}^{i}D_{1+j+\sum_0^i n}\left(\frac{T}{T_{\max}}\right)^{i-j}\left(\frac{n}{n_{\max}}\right)^{j} \quad (6)$$

In (6), η is the working efficiency of the motor, $D_{1+j+\sum_0^i n}$ is the fitting coefficient, T is the output torque, T_{max} is the maximum output torque, n is the output speed of the driving motor, and n_{max} is the highest output speed of the driving motor; the efficiency of the motor is illustrated in Fig. 6.

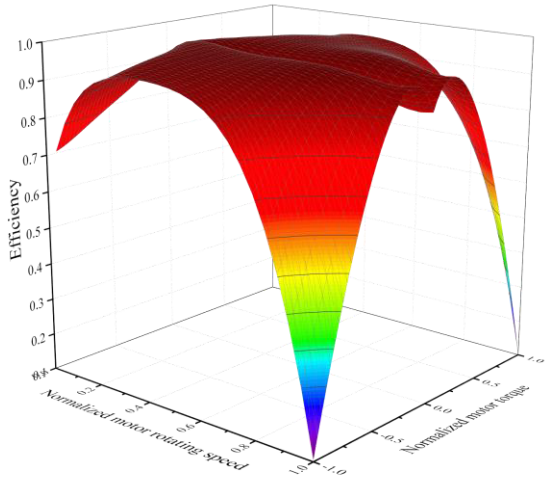

FIGURE 6. Normalized motor efficiency diagram.

E. DC/DC MODELS

Because of the different charging and discharging characteristics of the battery and the ultracapacitor, there exists a possibility of voltage mismatch (voltage clamping) in the direct parallel connection of the two, which puts HESS at a disadvantage. In this study, we use a bi-directional DC/DC converter, which controls the transfer power and regulates the voltage. Given that there will be energy loss in the transmission process of the DC/DC converter, the efficiency effect must be considered in the power system of the HESS.

F. BUSBAR POWER BALANCE MODEL

The demand power of the vehicle is expressed as follows:

$$P_d=\frac{v}{3600\eta_t}\left(mgf\cos\alpha+\frac{C_D A v^2}{21.15}+mg\sin\alpha+\delta m\frac{dv}{dt}\right) \quad (7)$$

The power balance of the demand power and dc busbar is,

$$P_d=\begin{cases}P_{HESS}/\eta_{reg} & charge\\ P^*_{HESS}\eta_e & discharge\end{cases} \quad (8)$$

The power balance between the dc busbar and the power source is as follows:

$$P_{HESS}=\begin{cases}P_{b,out}+P^*_{c,out}\eta_{DC} & P_{c,out}\geq 0\\ P_{b,out}+P_{c,out}/\eta_{DC} & P_{c,out}<0\end{cases} \quad (9)$$

In the above equations, P_d is the whole vehicle demand power, v is the vehicle speed, M is the mass of the electric vehicle, g is the acceleration due to gravity, f is the coefficient of rolling resistance, and α is the slope of the road (in this paper, α=0). C_D is the drag coefficient of air and A is the windward area; δ is the conversion factor of the vehicle rotation mass, P_{HESS} is the power of the HESS, η_t is the transmission system efficiency, η_{DC} is the DC/DC converter efficiency, η_e is the motor efficiency, and η_{reg} is the brake energy recovery efficiency.

III. PRELIMINARY PARAMETER MATCHING

Before the configuration of the HESS can be determined, it is necessary to undertake preliminary matching between the battery and the ultracapacitor in the system to enable the HESS to meet the energy and power requirements of the vehicle.

A. BATTERY PARAMETERS

The motor parameters used in the HESS are listed in Table 1. The voltage of the battery is determined by the motor voltage level, and the number of battery monomers in series is given by (10):

$$n_{bs}=\frac{u_{e\_nom}}{u_{b\_cell}} \quad (10)$$

where n_{bs} is the number of battery monomers in series, u_{b_cell} is the battery voltage, and u_{e_nom} is the motor rated voltage. The number of battery units is rounded off to 96. The number of parallel connections is determined based on the range of the electric vehicle. The maximum range is 150 km (cruising speed is 60 km/h). Because the power demand is more stable at constant speed, the battery is the only energy source. The maximum range for the electric vehicle is given by the following expression:

$$M_R\leq\frac{n_{bs}n_{bp}u_{b\_cell}Q_{b\_cell}\eta_e\eta_t}{1000(mgf+C_D A v_0^2/21.15)} \quad (11)$$

where n_{bp} is the number of battery units connected in parallel and v_0 is the speed at the maximum range. Considering

TABLE 1. Parameters of vehicle permanent magnet synchronous motor.

Motor parameters	Numerical value
Peak power (kW)	120
Rated Power (kW)	55
peak torque (Nm)	300
Rated torque (Nm)	120
Rated voltage (V)	350

the cost, the number of battery units is rounded off to one. Thus, the battery is made up of 96 cells in series. During the simulation, the initial charge state BSOC was set to 0.7.

B. ULTRACAPACITOR PARAMETERS

Compared with battery parameter matching, ultracapacitor group parameter matching is relatively more complicated. Given that the multiplication factor of DC/DC is generally not greater than four [19], the minimum voltage of the ultracapacitor is 350/4 = 87.5 V. Ultracapacitors release 75% of their energy when discharging from maximum voltage uc_{max} to 1/2 uc_{max}. In practical applications, if the lowest working voltage is half of its maximum voltage, then the maximum voltage of the ultracapacitor is $uc_{max} = 87.5\times2 = 175$ V. The number of ultracapacitor units in series is given by (12):

$$n_{cs} = \frac{u_{c\max}}{u_{c\_cell\_\max}} \tag{12}$$

where $u_{c\_cell\_max}$ is the upper limit of the voltage of the ultracapacitor unit. (Note that n_{cs} was rounded off to 65.) The power required for a vehicle to travel at a constant speed is termed the average power, which is given by (13):

$$P_{average} = \frac{v}{3600\eta_t}(mgf + \frac{C_D A v^2}{21.15}) \tag{13}$$

where $P_{average}$ is the average power for the battery, and the driving speed v is 60 km/h. In order to obtain more appropriate parameters for the optimization problem, ultracapacitors should meet the power requirements beyond the average power of the battery, and not be limited to new European driving cycle (NEDC) conditions. The difference between the peak power of the motor and the average power of the battery is referred to as the power demand of the ultracapacitor. Therefore, to meet the demand of $t_p = 10$ s of peak power, the number of ultracapacitor units that need to be connected in parallel is calculated using (14):

$$\begin{cases} \Delta E_c = \int_{t_0}^{t_0+t_p} [P_{e\_\max}(t) - P_{average}(t_0)]dt \\ n_{cp} = \dfrac{8\Delta E_c}{3n_{cs}u^2_{c\_cell\_\max}C_{c\_cell}} \end{cases} \tag{14}$$

In the above expression, ΔE_c is the ultracapacitor energy demand, P_{e_max} is the motor peak power (120 kW), and $P_{average}$ is the average power provided by the battery, as obtained using (13). n_{cp} is the number of ultracapacitor units connected in parallel, and C_{c_cell} is the capacity of each ultracapacitor unit. The number of ultracapacitor units connected in parallel in the above equation is rounded off to three. Thus, three groups of 65 ultracapacitor monomers are connected in parallel. In the simulation process, the USOC was set to 0.7 when the ultracapacitor was in the initial state of charge.

IV. PSEUDOSPECTRAL OPTIMIZATION METHOD

In the developed optimization strategy, first the Radau pseudospectral method is used to separate the discrete state variables and control variables. Then, a Lagrange interpolation polynomial is applied to approximate the state and control variables. The differential operation in the state equation and integral operation in the performance function are then transformed into algebraic operations. Finally, the optimal control problem (OCP) is transformed into a nonlinear programming (NLP) problem in which the state variable at the node and the control variable at the collocation point are the parameters to be optimized. The steps involved in the optimization are as follows:

Let the driving process of a HESS electric vehicle be divided into Q stages under NEDC working cycles. The initial time point and the ensuing Q-1 subsection points are recorded as T_0, T_1,..., T_Q, and T_0<T_1<...< T_Q.

(1) Time-domain transformations convert each period $[T_{q-1}, T_q]$ (where q $\in$1, q $\cap Z^+$) in the whole time-domain to interval [-1, 1], such that the definition interval of the Legendre orthogonal polynomial is satisfied:

$$\tau = \frac{2t - (T_q + T_{q-1})}{T_q - T_{q-1}}, \quad \tau \in [-1, 1] \tag{15}$$

(2) Collocation point and discretization: The collocation point of the Radau pseudospectral method is the Legendre-Gauss-Radau (LGR) point, i.e., the value interval is $\tau\in(-1, 1]$ or $\tau \in [-1, 1)$. In this study, we select $\tau \in (-1, 1]$ as the collocation interval, which is the root of $P_N(\tau) - P_{N-1}(\tau)$. $P_N(\tau)$ is the N^{th} Legendre orthogonal polynomial, which is given by (16):

$$P_N(\tau) = \frac{1}{2^N N!}\frac{d^N}{d\tau^N}[(\tau^2 - 1)^N], \quad N = 0, 1, 2, \ldots \tag{16}$$

The nodes of the Radau pseudospectral method are N *LGR* collocation points and initial time points $\tau_0 = -1$. Therefore, the number of nodes is N+1. For pseudo spectral mosaics with Q stages, the number of nodes in each stage, which can differ, is recorded as N_q+1; the node in the Q phase is marked as $\tau_{q,i}$, where i = 0, 1 ,..., N_q. The BSOC and USOC are taken as state variables in the simulation process. The state variables in each stage are discretized at the nodes, and can be expressed as follows:

$$\begin{cases} BSOC_q = [BSOC_{q,0}\ BSOC_{q,1}\ \cdots\ BSOC_{q,N_q}] \\ USOC_q = [USOC_{q,0}\ USOC_{q,1}\ \cdots\ USOC_{q,N_q}] \end{cases} \tag{17}$$

Then, the time history curve of the state variables in each stage can be approximated by N_q+1 Lagrange interpolating polynomials as follows:

$$\begin{cases} BSOC_q(\tau) \approx \sum_{i=0}^{N_q} L_{q,i}(\tau) BSOC_{q,i} \\ USOC_q(\tau) \approx \sum_{i=0}^{N_q} L_{q,i}(\tau) USOC_{q,i} \end{cases} \tag{18}$$

Here, $L_{q,i}(\tau)$ is the base function of the N_q degree sub-Lagrange interpolation, which is given by

$$L_{q,i}(\tau) = \prod_{j=0, j\neq i}^{N_q} \frac{\tau - \tau_{q,j}}{\tau_{q,i} - \tau_{q,j}} \tag{19}$$

The battery power $P_{b,out}$ are used as the control variables in the optimization process. They are discretized only at the collocation point. Thus, the control variables in each stage can be expressed as follows:

$$P_{b,out_q} = [P_{b,out_{q,1}}\ P_{b,out_{q,2}}\ \cdots\ P_{b,out_{q,N_q}}] \tag{20}$$

Then, the time history curves of the control variables can be approximated by N_q Lagrange interpolating polynomials in each stage as follows:

$$P_{b,out_q}(\tau) \approx \sum_{i=1}^{N_q} \tilde{L}_{q,i}(\tau) P_{b,out_{q,i}} \tag{21}$$

Here, $\tilde{L}_{q,i}(\tau)$ is the base function for the N_{q-1} degree Lagrange interpolation, which is expressed as follows:

$$\tilde{L}_{q,i}(\tau) = \prod_{j=1,j\neq i}^{N_q} \frac{\tau - \tau_{q,j}}{\tau_{q,i} - \tau_{q,j}} \tag{22}$$

(3) The state equation is transformed into an algebraic constraint, and after collocation and discretization, the state variables are approximated by the global interpolating polynomials. Thus, the differentiation operation can be expressed as the derivation of the interpolating polynomials in (18), as follows:

$$\begin{cases} \dot{BSOC}_q(\tau_{q,k}) = \sum_{i=0}^{N_q} \dot{L}_{q,i}(\tau_{q,k}) \cdot BSOC_{q,i} = \sum_{i=0}^{N_q} D_{ki}^q \cdot BSOC_{q,i} \\ \dot{USOC}_q(\tau_{q,k}) = \sum_{i=0}^{N_q} \dot{L}_{q,i}(\tau_{q,k}) \cdot USOC_{q,i} = \sum_{i=0}^{N_q} D_{ki}^q \cdot USOC_{q,i} \end{cases} \tag{23}$$

where $\tau_{q,k}$ is the collocation point in phase q, where $k = 1,2,\ldots,N_q$; D_{ki}^q is the differential matrix of $N_q \bullet (N_q + 1)$, which represents the differential value of the basis function of Lagrange interpolation in phase q at each collocation point;

D_{ki}^q is expressed as follows:

$$D_{ki}^q = \dot{L}_i(\tau_k) = \begin{cases} \dfrac{\ddot{g}(\tau_{q,i})}{2\dot{g}(\tau_{q,i})} & i = k \\ \dfrac{\dot{g}(\tau_{q,k})}{\dot{g}(\tau_{q,i})(\tau_{q,k} - \tau_{q,i})} & i \neq k \end{cases} \tag{24}$$

where $\mathrm{g}\left(\tau_{q,i}\right) = \left(1 + \tau_{q,i}\right)\left[P_{N_q}\left(\tau_{q,i}\right) - P_{N_{q-1}}\left(\tau_{q,i}\right)\right]$

The first-order differential of the charge state BSOC to time, which is obtained from (1) and (2), is expressed as follows:

$$\dot{BSOC} = -\frac{u_b(BSOC(t)) - \sqrt{u_b^2(BSOC(t)) - 4P_{b,out}(t)R_b(BSOC(t))}}{2R_b(BSOC(t))Q_b} \tag{25}$$

The first-order differential of the ultracapacitor state USOC to time, from (3), (4), (5), and (9), is expressed in (26), as shown at the bottom of this page, where *sign* is a sign function. Combined with (23), (24), (25), and (26), the energy management optimal control problem of the HEV is transformed in phase q from a dynamic equation constraint into an algebraic constraint at collocation point $\tau_{q,k}$: as given in (27) and (28), as shown at the bottom of this page.

(4) Transformation of performance function in the multi-objective energy management optimal control problem of hybrid power vehicles mainly focuses on the performance index, which consists of *Aheff* and HESS energy consumption (E_{HESS}). To avoid a large current discharge, penalty factors are added into the battery in the Ah-throughput of the battery [19]. The objective function thus obtained is expressed as in (29):

$$\begin{cases} Aheff(t) = \int_0^{t_f} \sigma(t)|i_b(t)|dt \\ E_{HESS}(t) = \dfrac{1}{2}C_c u_{\max}^2 \Delta USOC(t)^2 + \int_0^{t_f} i_b(t) * u_b(t)dt \\ J = Aheff + E_{HESS} \end{cases} \tag{29}$$

where σ is the penalty factor, and its main determinant factor depends on the charge-discharge ratio i_c, temperature, and discharge depth, which can be simplified to (30):

$$\begin{cases} \sigma(t) = \dfrac{1.6}{625} i_c^2(t) + 1 \\ i_c(t) = \dfrac{i_b(t)}{Q_b} \end{cases} \tag{30}$$

In the above expression, i_b is the charge and discharge current and Q_b is the rated capacity of the battery. The performance functions contain both non-integral (Mayer-type

$$\dot{USOC} = -\frac{USOC(t) * u_{c\max} - \sqrt{(USOC(t) * u_{c\max})^2 - 4\left(\frac{P_{HESS}(t) - P_{b,out}(t)}{\eta_{DC} \wedge sign(P_{c,out}(t))}\right)R_c}}{2R_c C_c u_{c\max}} \tag{26}$$

$$\sum_{i=0}^{N_q} D_{ki}^q \cdot BSOC_{q,i} = \frac{T_q - T_{q-1}}{2} \frac{\sqrt{u_b^2(BSOC_{q,k}) - 4P_{b,out}(\tau_{q,k})R_b(BSOC_{q,k})} - u_b(BSOC_{q,k})}{2Q_b R_b(BSOC_{q,k})} \tag{27}$$

$$\sum_{i=0}^{N_q} D_{ki}^q \cdot USOC_{q,i} = \frac{T_q - T_{q-1}}{2} \frac{\sqrt{\left(USOC(\tau_{q,k}) * u_{c\max}\right)^2 - 4\left(\frac{P_{HESS}(\tau_{q,k}) - P_{b,out}(\tau_{q,k})}{\eta_{DC} \wedge sign(P_{c,out}(\tau_{q,k}))}\right)R_c} - USOC(\tau_{q,k}) * u_{c\max}}{2C_c u_{c\max} R_c} \tag{28}$$

performance index) and integral term (Lagrange-type performance index), which can be optimized using the Gauss–Radau integral method, which approximates its integral term. Thus, the objective function obtained is given as follows:

$$J_q = \frac{1}{2}C_c u_{c\max}^2 \Delta USOC^2 + \frac{T_q - T_{q-1}}{2} \times \sum_{k=1}^{N_q} \omega_{q,k}\sigma(\tau_{q,k})|i_b(\tau_{q,k})| + i_b(\tau_{q,k})u_b(\tau_{q,k}) \quad (31)$$

where $\omega_{q,k}$ is the integral weight, which is expressed as follows:

$$\omega_{q,k} = \frac{1-\tau_{q,k}}{N_q^2 \cdot [P_{N_q-1}(\tau_{q,k})]^2} \quad (32)$$

(5) Through the above five steps, the optimal control problem of multi-objective energy management for the original HESS can be transformed into an NLP problem with optimization variables:

$$min\ J = \frac{1}{2}C_c u_{c\max}^2 \Delta USOC^2 + \sum_{q=1}^{Q} \frac{T_q - T_{q-1}}{2} \sum_{k=1}^{N_q} \omega_{q,k}\sigma|\ i_b\ | + i_b u_b \quad (33)$$

The state equation is given in (27) and (28), where the constraints are as follows:

$$\begin{cases} BSOC_{\min} \le BSOC(t) \le BSOC_{\max} \\ P_{b,out\_\min} \le P_{b,out}(t) \le P_{b,out\_\max} \\ USOC_{\min} \le USOC(t) \le USOC_{\max} \\ P_{c,out\_\min} \le P_{c,out}(t) \le P_{c,out\_\max} \end{cases} \quad (34)$$

In the NLP problem, the variables to be optimized are the BSOC, USOC, and output power of the battery $P_{b,Out}$ at the LGR point, which can be solved using a mature high-dimensional sparse NLP solver. The sparse nonlinear optimizer (SNOPT) is a sequential quadratic programming method based on line search with local superlinear convergence.

V. PARAMETER SETTINGS AND OPTIMIZATION RESULTS

A. OPTIMIZING PARAMETER SETTINGS

The parameters in the optimization process are shown in Table 2, where v represents the speed, in km/h. In this study, the NEDC condition was used to optimize the simulation. Based on the demand power of the vehicle, the driving conditions of the vehicle were categorized into power rising stage (acceleration condition), power maintaining stage (uniform speed condition), power negative stage (deceleration condition), and power zero. In an electric vehicle with HESS, the acceleration condition is supplied by the battery and the capacitor together. However, the energy is supplied by the battery under uniform conditions. The energy generated by braking is recovered by the preferred capacitance in the decelerating condition; when the power is zero, neither the battery nor the capacitor is engaged. Moreover, given the complexity of the whole NEDC stage, the number of stages is significantly large (69 stages in total). Hence, based on the pseudospectral optimization method, this paper divides the suburban working conditions into 12 stages, as shown in Table 3, by taking the suburban working conditions as an example.

TABLE 2. Simulation parameters.

Parameter	Numerical value
Vehicle mass, *m (kg)*	1645
Glide mass (Glide resistance parameter) (kg)	1710
Wheel radius, *r (m)*	0.317
Sliding resistance curve, *F (N)*	F=0.0353 × v2+1.4114 × v+114.7712
Rolling resistance factor, *f*	0.01
Drag coefficient of air, *CD*	0.29
Windward area, A/m^2	2.09
Rotational mass coefficient, δ	1.05
Transmission efficiency, ηt	0.965
Motor to wheel speed ratio, *im*	7.741
Brake energy recovery efficiency, η_{reg}	0.4
DC/DC efficiency, ηDC	0.9
Battery capacity, Q_{b_cell} (Ah)	37
Battery nominal voltage, u_{b_cell} (V)	3.65
Minimum charge state of battery, $BSOC_{min}$	0.2
Maximum charge status of battery, $BSOC_{max}$	0.9
Ultracapacitor capacity, C_{c_cell} (F)	3000
Maximum voltage of the ultracapacitor, $u_{c\_cell\_max}$ (V)	2.7
Ultracapacitor internal resistance, R_{c_cell} (Ω)	0.00029
Lower limit of capacitance charge, $USOC_{min}$	0.4
Maximum capacitance charge, $USOC_{max}$	0.95

B. OPTIMIZED RESULTS

Fig. 7 shows the optimization results of the Radau pseudospectral method in NEDC. The relationship between the energy consumption of the HESS system and the Ah-throughput of the battery is obtained. In the Pareto optimal solution set, as indicated by the red data points in the figure, when the Ah-throughput of the battery decreases, the power and current of the battery are relatively low, and hence capacitance consumes more energy. In contrast, when the energy consumption of the HESS decreases, the power and

TABLE 3. Stage classification of NEDC suburban working cycles.

Time interval (s)	Mode	Time interval (s)	Mode
[800,840]	Accelerating mode	[1030,1065]	Accelerating mode
[840,890]	Maintaining constant speed mode	[1065,1095]	Maintaining constant speed mode
[890,898]	Decelerating mode	[1095,1115]	Accelerating mode
[898,967]	Maintaining constant speed mode	[1115,1125]	Maintaining constant speed mode
[967,980]	Accelerating mode	[1125,1159]	Decelerating mode
[980,1030]	Maintaining constant speed mode	[1159,1180]	Zero power

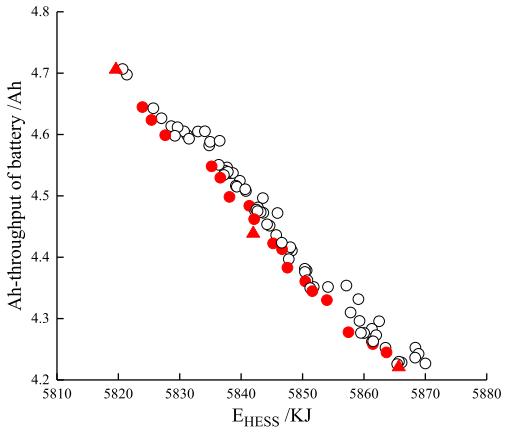

FIGURE 7. Multi-objective optimization results under NEDC conditions.

current of the battery increases accordingly, and the capacitor energy consumption decreases.

According to the definition of the Pareto front solution set, the relationship between every two points in the graph is nondominant; in other words, a reduction in either the target energy consumption of HESS or the Ah-throughput of the battery will lead to deterioration of the other target. Therefore, in this study, three representative groups of data were selected for analysis. The three red triangles shown in Fig. 7 are the HESS minimum energy consumption point, the balanced tradeoff optimal solution point, and the battery longest equivalent lifetime point, respectively.

Figs. 8 and 9 show the SOC variation curves and power flow diagrams between the two energy sources with the smallest energy consumption of the HESS. Figs. 10 and 11 show the SOC variation curves and power flow diagrams between the two energy sources with the longest equivalent life of the battery. As the life of the battery is prolonged, the energy consumption of the system increases slightly, and a group of data with longer battery equivalent lifetime is selected as the balanced tradeoff optimal solution. Figs. 12 and 13 show the balanced tradeoff optimal solution of the SOC variation curve and the power flow diagram between the two selected energy sources. Figs. 14 and 15 show SOC variation curves and power flow diagrams for a single battery energy source.

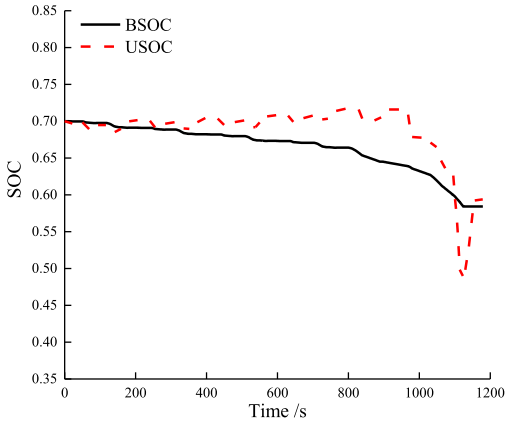

FIGURE 8. SOC optimization result of HESS minimum energy consumption.

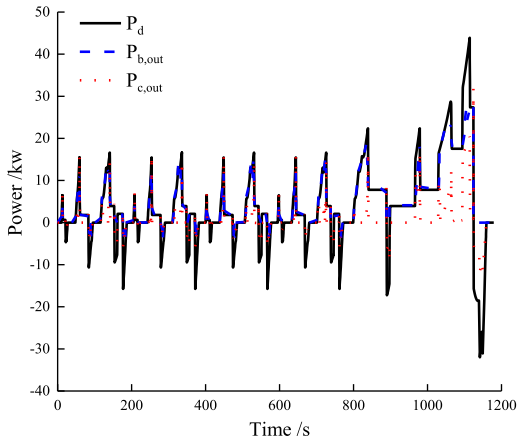

FIGURE 9. Power optimization result of HESS minimum energy consumption.

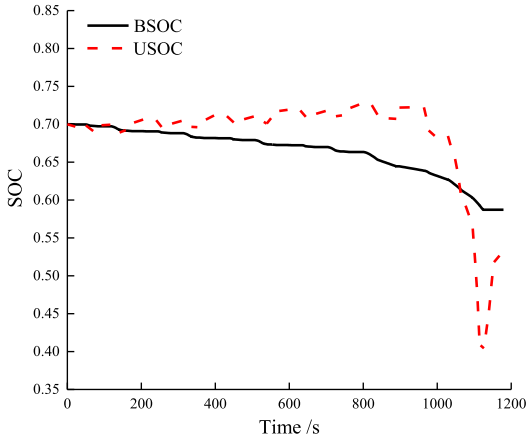

FIGURE 10. SOC optimization results when the battery has the longest equivalent lifetime.

In the post-Pareto solution set, the energy consumption of the HESS increases with increase in the Ah-throughput of the battery. This behavior can be attributed to the fact that, in addition to meeting the demand power of the vehicle, the flow of energy within the system between the two energy sources is increased. Moreover, the Ah-throughput of the battery is

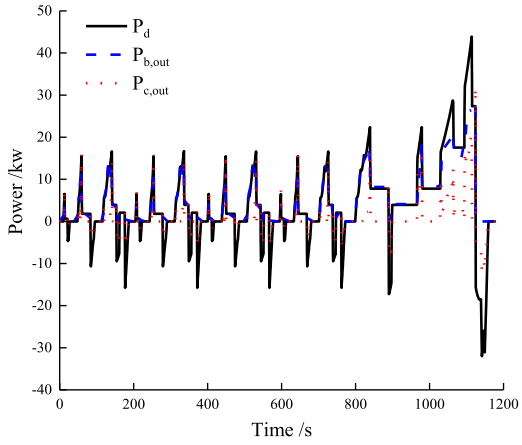

FIGURE 11. Power optimization result when the battery has the longest equivalent lifetime.

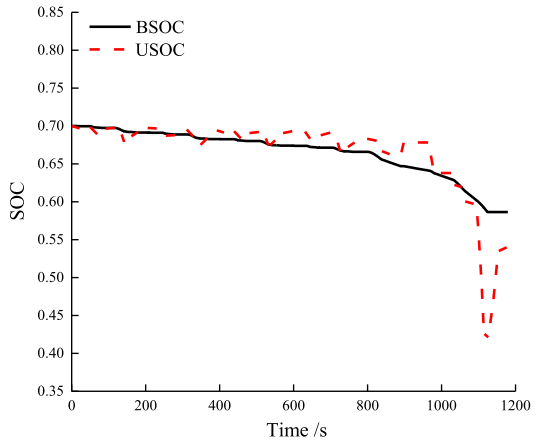

FIGURE 12. SOC optimization results for balanced tradeoff optimal solution.

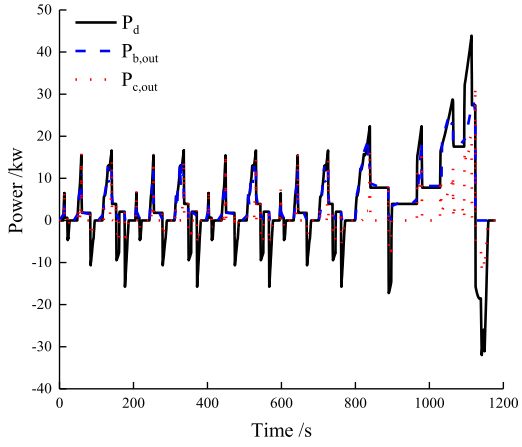

FIGURE 13. Power optimization result of balanced tradeoff optimal solution.

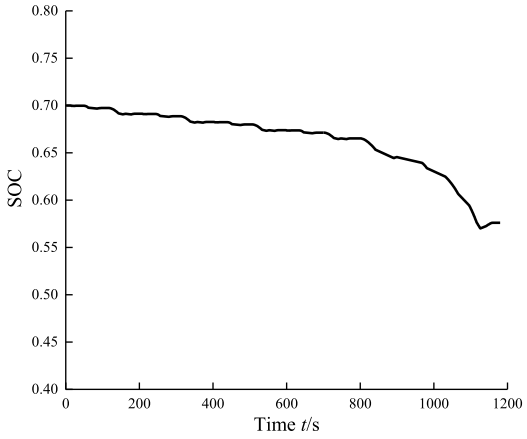

FIGURE 14. Simulation results of single battery SOC.

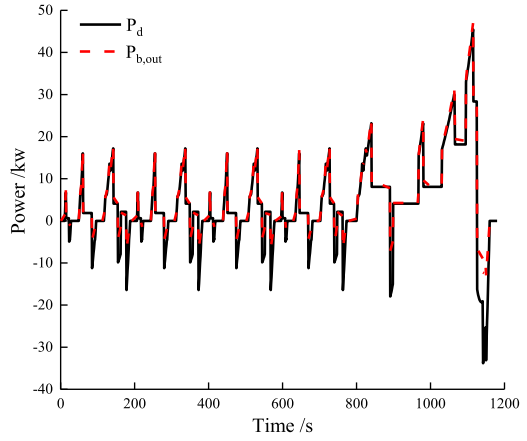

FIGURE 15. Simulation result of single battery power.

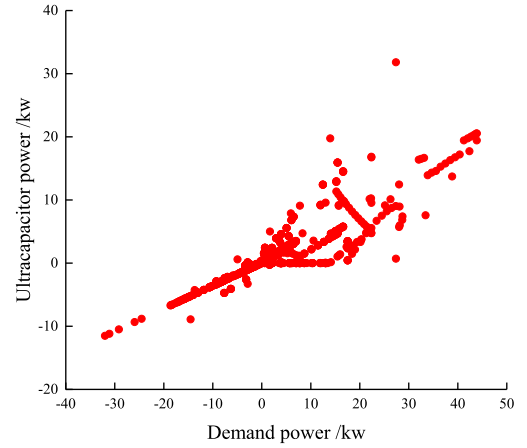

FIGURE 16. Ultracapacitor power distribution diagram.

also increased, leading to simultaneous deterioration of the two targets.

Figs. 16 and 17 illustrate the relationship between ultracapacitor power and demand power, and battery power and demand power in the HESS. It can be seen that the demand power is negative in the deceleration stage. In addition, the power is absorbed by the ultracapacitor, and the battery provides a maximum of 5 kW of power for the ultracapacitor. In addition, the required power in the constant speed phase is only provided by the battery, and the uniform power includes 0.8 kW, 2 kW, 4 kW, 7.3 kW, 14 kW, 22 kW. The acceleration phase, when the required power is between 0–20 kW, can be

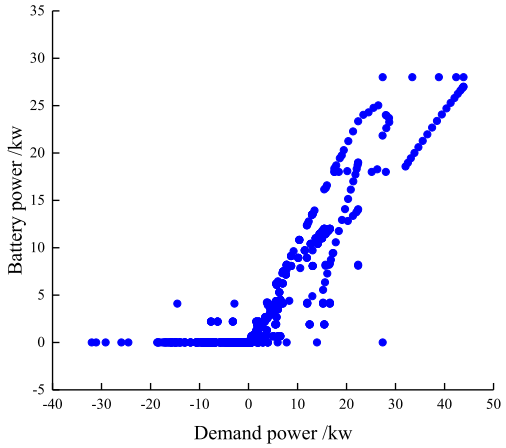

FIGURE 17. Battery power distribution diagram.

further divided into two phases. One phase is the linear relationship between the power of the battery and the demand power for the long-term large demand power phase. The other phase is the short-term small demand power phase, which is supplemented by the ultracapacitor. The above optimization results show the characteristics of rapid charging and discharging of the ultracapacitor. The pseudospectral method divides the working condition into multiple stages. Therefore, when the acceleration stage is transformed into other stages, a sudden change in the power of the battery forces the ultracapacitor to supplement the decrease in power. When the ultracapacitor is drained, the required power is solely supplied by the battery.

In this paper, the battery Ah-throughput is converted into the battery equivalent lifetime. The equation for calculating the battery equivalent lifetime is given by (35) [20]:

$$L = \frac{\Gamma}{Aheff} = \frac{20000 \times 3600 \times Q_b}{2.3 \times Aheff} \tag{35}$$

where Γ is the total Ah-throughput of the battery; its value is determined by the battery, and it remains constant. When $\Gamma = Aheff$, the battery reaches its lifetime limit. L represents the equivalent battery life. In addition, this study also expressed the number of battery cycles in NEDC conditions. The optimized results of three datasets show that the minimum energy consumption of the HESS can reach 5819.60 kJ, with the equivalent life of the battery at 68368 cycles. Moreover, the maximum equivalent life of the battery can reach 76227 cycles when the energy consumption of the HESS is 5865.68 kJ. As regards the balanced tradeoff optimal solution, the equivalent life of the battery of the optimal solution is 72488 cycles, with the energy consumption of the HESS at 5841.96 kJ. In contrast, the equivalent life of the single-cell energy source is 55796 cycles, with an energy consumption of 5948.3 kJ.

VI. CONCLUSION

In this study, a multi-objective optimization method based on the Radau pseudospectral method was used to optimize the energy management strategy of the hybrid electric vehicle, with the system energy consumption and lifetime of the battery considered as the optimization objectives. In the battery models, the internal resistance characteristics of the battery during charging and discharging were taken into account.

Optimized results were obtained in a Pareto solution set. Three solutions representing different tradeoffs were selected for further analysis: minimum system energy consumption (5819.60 kJ), with battery life 68368 cycles; maximum battery life (76227 cycles), with energy consumption 5865.68 kJ; and a balanced tradeoff optimal solution with battery life 72488 cycles and energy consumption 5841.96 kJ. For every additional 5 kJ in system energy consumption, the battery Ah-throughput was reduced by 0.053 Ah and its equivalent life extended by 876 cycles. Compared with the single-cell energy source, the balanced tradeoff optimal solution increased the battery life by 29.92% and decreased the system energy consumption by 1.79%.

This study provides a fast and stable multi-objective optimization method for the energy management strategy of HESS. The proposed method also provides a basis for matching the optimal parameters of HESS and a reference for the formulation of an online energy management strategy.

REFERENCES

[1] L. Zhang, X. Hu, Z. Wang, F. Sun, J. Deng, and D. G. Dorrell, "Multiobjective optimal sizing of hybrid energy storage system for electric vehicles," *IEEE Trans. Veh. Technol.*, vol. 67, no. 2, pp. 1027–1035, Feb. 2018.

[2] Z. Y. Song, J. Li, X. Han, L. Xu, L. Lu, M. Ouyang, and H. Hofmann, "Multi-objective optimization of a semi-active battery/supercapacitor energy storage system for electric vehicles," *Appl. Energy*, vol. 135, pp. 212–224, Dec. 2014.

[3] M.-E. Choi, J.-S. Lee, and S.-W. Seo, "Real-time optimization for power management systems of a battery/supercapacitor hybrid energy storage system in electric vehicles," *IEEE Trans. Veh. Technol.*, vol. 63, no. 8, pp. 3600–3611, Oct. 2014.

[4] X. Wu, W. Hou, and Z. Shuai, "Research on energy management of hybrid energy storage system for electric bus," *Adv. Mech. Eng.*, vol. 9, no. 10, pp. 1–13, 2017.

[5] C. Wang, B. Huang, and W. Xu, "An integrated energy management strategy with parameter match method for plug-in hybrid electric vehicles," *IEEE Access*, vol. 6, pp. 62204–62214, 2018.

[6] X. Lu, Y. Chen, M. Fu, and H. Wang, "Multi-objective optimization-based real-time control strategy for battery/ultracapacitor hybrid energy management systems," *IEEE Access*, vol. 7, pp. 11640–11650, Feb. 2019.

[7] A. Santucci, A. Sorniotti, and C. Lekakou, "Power split strategies for hybrid energy storage systems for vehicular applications," *J. Power Sour.*, vol. 258, pp. 395–407, Jul. 2014.

[8] F. Zhou, F. Xiao, C. Chang, Y. Shao, and C. Song, "Adaptive model predictive control-based energy management for semi-active hybrid energy storage systems on electric vehicles," *Energies*, vol. 10, no. 7, p. 1063, 2017.

[9] Z. Song, H. Hofmann, J. Li, X. Han, and M. Ouyang, "Optimization for a hybrid energy storage system in electric vehicles using dynamic programing approach," *Appl. Energy*, vol. 139, pp. 151–162, Feb. 2015.

[10] J. Peng, H. He, and R. Xiong, "Rule based energy management strategy for a series–parallel plug-in hybrid electric bus optimized by dynamic programming," *Appl. Energy*, vol. 185, pp. 1633–1643, Jan. 2017.

[11] S. Zhang, R. Xiong, and J. Cao, "Battery durability and longevity based power management for plug-in hybrid electric vehicle with hybrid energy storage system," *Appl. Energy*, vol. 179, pp. 316–328, Oct. 2016.

[12] D. Xu, Q. Liu, X. Yan, and W. Yang, "Adaptive terminal sliding mode control for hybrid energy storage systems of fuel cell, battery and supercapacitor," *IEEE Access*, vol. 7, pp. 29295–29303, 2019.

[13] H. He, R. Xiong, K. Zhao, and Z. Lium "Energy management strategy research on a hybrid power system by hardware-in-loop experiments," *Appl. Energy*, vol. 112, no. 16, pp. 1311–1317, 2013.
[14] G. Elnagar, M. A. Kazemi, and M. Razzaghi, "The pseudospectral Legendre method for discretizing optimal control problems," *IEEE Trans. Autom. Control*, vol. 40, no. 10, pp. 1793–1796, Oct. 1995.
[15] S. Wei, Y. Zou, F. Sun, and O. Christopher, "A pseudospectral method for solving optimal control problem of a hybrid tracked vehicle," *Appl. Energy*, vol. 194, pp. 588–595, May 2017.
[16] J. Ye, K. Zhao, Y. Liu, X. Huang, and H. Lin, "Multi-stage global trajectory optimization for the overlapping shift of a seamless two-speed transmission using Legendre pseudo-spectral method," *Adv. Mech. Eng.*, vol. 9, no. 12, pp. 1–13, 2017.
[17] AW. Zhou, C. Zhang, J. Li, and H. K. Fathy, "A pseudospectral strategy for optimal power management in series hybrid electric powertrains," *IEEE Trans. Veh. Technol.*, vol. 65, no. 6, pp. 4813–4825, Jun. 2016.
[18] L. Guo, B. Gao, H. Chen, and J. Lu, "On-line shift schedule optimization of electric vehicles with multi-speed AMT using moving horizon strategy," in *Proc. 34th Chin. Control Conf.*, Jul. 2015, pp. 8097–8102.
[19] A. M. Jarushi and N. Schofield, "Battery and supercapacitor combination for a series hybrid electric vehicle," in *Proc. 5th IET Int. Conf. Power Electron., Mach. Drives (PEMD)*, Apr. 2010, pp. 1–6.
[20] K. Zhao, Z. Liang, Y. Huang, H. Wang, A. Khajepour, and Y. Zhen, "Research on a novel hydraulic/electric synergy bus," *Energies*, vol. 11, no. 1, p. 34, 2018.

YANWEI LIU received the Ph.D. degree in vehicle engineering from the South China University of Technology, Guangzhou, China, in 2012. He is currently with the Guangdong University of Technology. His current research interests include energy management strategy of hybrid energy storage systems and multi-objective optimization of nonlinear dynamic systems.

ZHENYE LI received the B.S. degree in vehicle engineering from the Dongguan University of Technology, Dongguan, China, in 2018. He is currently pursuing the M.S. degree in vehicle engineering with the Guangdong University of Technology, Guangzhou, China. His current research interest includes energy management strategy of hybrid energy storage systems.

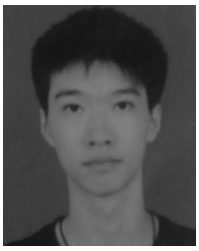

ZIYUE LIN received the B.S. degree in vehicle engineering from the Guangdong University of Technology, Guangzhou, China, in 2017, where he is currently pursuing the M.S. degree in vehicle engineering. His current research interest includes multi-objective optimization of nonlinear dynamic systems.

KEGANG ZHAO received the B.S. degree in automotive engineering and the Ph.D. degree in vehicle engineering from the South China University of Technology, Guangzhou, China, in 1999 and 2005, respectively. Since 2005, he has been with the School of Mechanical and Automotive Engineering, South China University of Technology, where he is currently an Associate Professor of vehicle engineering. His current research interests include hybrid power electric vehicle, design, and control of advanced transmission.

YUNXUE ZHU received the B.S. degree from the Hebei University of Engineering, Hebei, China, in 2016, and the M.S. degree from the Guangdong University of Technology, Guangzhou, China, in 2019, both in vehicle engineering. His current research interest includes energy management strategy of hybrid energy storage systems.